POLITECNICO
MILANO 1863

DIPARTIMENTO DI MECCANICA

mecc

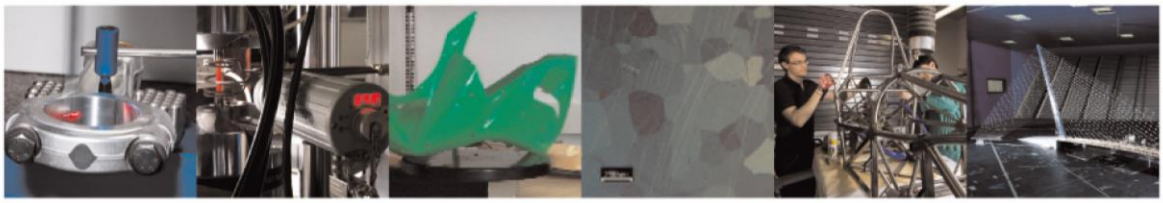

On the use of effective thermophysical properties to predict the melting process of composite phase change materials with coarse structures

Ziwei Li, Elisabetta Gariboldi

This is a post-peer-review, pre-copyedit version of an article published in journal title. The final authenticated version is available online at:
https://doi.org/10.1016/j.ijheatmasstransfer.2021.121765

DIPARTIMENTO DI MECCANICA ■ POLITECNICO DI MILANO
via G. La Masa, 1 ■ 20156 Milano ■ EMAIL (PEC): pecmecc@cert.polimi.it
http://www.mecc.polimi.it

Rev. 0

n the use of effective thermophysical properties to predict the melting process of composite phase change materials with coarse structures

Ziwei Li[a], Elisabetta Gariboldi[b]

[a]Politecnico di Milano, Department of Mechanical Engineering, Via La Masa 1, 20156 Milan, Italy. E-mail address: ziwei.li@polimi.it (Z. Li). ORCID: 0000-0001-6878-2246

[b]Corresponding author at: Politecnico di Milano, Department of Mechanical Engineering, Via La Masa 1, 20156 Milan, Italy. E-mail address: elisabetta.gariboldi@polimi.it (E. Gariboldi). ORCID: 0000-0002-4443-3495

Abstract

Composite PCMs combining metallic foam and paraffin are widely used as phase change materials (PCMs) to tailor the properties of pure PCMs and enhance the thermal energy storage/release. For the complex composites structures, the transient thermal response prediction by direct simulation (DS) is not easy in term of geometry generation and computation. The volume-averaged model (1T model) considering the composite PCMs as homogeneous media is sometimes used to deal with thermal transport in Composite PCMs, not always with a sufficiently good local description of non-steady conditions. The paper carries out a set of cases where a composite PCM modelled as an open-pore body-centred cell made of Aluminium (Al) filled with paraffin (i) to investigate the combined effects of the geometry of the unit cell (side length, porosity), the composite sample (sample height) and boundary conditions (heat input) on the heat response; (ii) to identify the local/overall errors in temperature and volume fraction of liquid PCM (and thus of stored heat) induced by the use of 1T model for various geometry/heat flux combinations. Analytical equations are proposed to predict the maximum temperature difference between Al and PCM as well as the maximum temperature difference calculated by applying 1T or DS model as a function of the open cell structure geometry and heat flux. The main novelty introduced in the paper is analytical model to quantify for 1T model the maximum local error on molten PCM volume fraction, and thus for heat stored/released. The model supplies good local thermal response predictions for fine structures and lower heat flux input. Nevertheless, errors in the volume fraction of molten PCMs predicted for the whole sample are far lower and the 1T model can be easily applied in a wider range of geometry/conditions.

Keywords

Composite Phase Change Material; effective thermophysical property; coarse structures; melting process.

1 Introduction

The phase change materials (PCMs) used in devices for thermal energy storage and management have been applied in biomedical, biomedical, electronic, textile, construction and automotive industries, but often suffer a limit for applicability due to their low thermal conductivity [1,2]. In order to overcome this defect, many researches on increasing thermal conductivity have carried out, such as micro-encapsulation techniques [1,3], foam-stable PCMs [1,4], metallic alloys [5,6].

Among these solutions, metal foams can have pore volume ranging in a wide range, so that the composite PCM which can be obtained by filling them by the material which activates the phase transition can correspondingly have a relatively large volume range of PCM. The foams are typically of metallic structures, specifically those characterized by high thermal conductivity, such as Al or Cu foam [7,8]. Many researchers have investigated the effect of metal foam as a means to increase the effective thermal conductivity of PCM composites. Xiao et al.[9] stated that the effective thermal conductivity of paraffin/copper foam characterized by 96.95%, 92.31%, 88.89% porosities foam are about 13, 31, 44 times larger than that of pure paraffin. Ren et al.[10] carried out a comparative study to evaluate the nanoparticle-metal foam combination on enhancing PCM melting, and thus its thermal storage performance. Their results indicated that, in view enhancing PCM heat transfer effectiveness, the use of metal foams is more effective than adding nanoparticles to PCM. Yang et al.[11] investigated the effect of inclination on the thermal response of pure paraffin and paraffin/copper foam (10 pores per inch and the porosity of 0.96). They reported that the inclination angle has little influence on the composite PCM since heat conduction dominates when the paraffin is melted in open-cell metal foam. The predominance of conductive heat transport over convective one in the temperature ranges where paraffin is molten has to be carefully considered for coarse structures and high porosity, as shown by the Li et al. in [12].

The prediction of the thermal response of PCM/metal foam composites is not always an easy task due to complex microstructure of foams. Therefore, direct numerical simulation (DS) is considered a more precise method to predict both general and local thermal response of PCM composites and in some cases they were reported to have some challenges as far as geometry generation and time cost are concerned [13,14]. In recent years, the volume-averaged

approaches like one-temperature (1T) [13–16] and two-temperature (2T) [13,14,17] models have been proposed and experimentally validated in order to save computational time. 1T model assumes that there is no temperature difference between foam and PCM while 2T model considers heat transfer between PCM and porous medium [13,14]. 1T model was used to predict the heat transfer behaviour in composite PCM/Cu foam system for the melting process [8]. The 1T model was also applied to describe the PCM solidification process in Cu [15] and multi-layer (Al, Cu and Ni) [16] open-cell metal foam. Hu et al. [13,14] stated that 1T model can describe the phase change behavior during heating in constant boundary conditions, in a PCM/Al foam system where the foam was represented as an ideal lattice made by Body-Centered Cubic (BCC) unit cells. Sardari et al.[18] claimed that 2T model can offer more accurate results compared with 1T model. However, some authors reported that 1T model can predict the identical results with 2T model [13,14] and agree reasonably well with experimental data [8,15,16].

Thus, summarizing the available scientific literature on it, among the two ‘simplified’ models, 1T model significantly simplifies the PCM/foam system by modelling it as a homogeneous material with effective thermal properties, which offers advantages of geometrical definition and computational cost for part design. Nevertheless, there is a lack of information on the foam size-dependence applicability of 1T model to PCM/metallic foams, where the temperature difference between the metal and PCM can become significantly high due to the low thermal diffusivity of PCM compared to that of the metallic phase of this composite. On the other hand 2T nodel requires the preliminar identification of parameters such as institution heat transfer coefficient and specific surface area which are related [13, 14] to the on the structural features which effect is to be addressed in the present paper. The 2T model has thus not been considered in the present paper.

The purpose of this paper is to investigate the effect of foam-size parameters as well as other parameter defining boundary conditions and to identify the errors induced by the use of 1T model in temperatures, volume fraction of molten phase. The models are applied under assumption of only conduction heat transfer. The 1T model predictions have been compared to those supplied by the computationally heavier Direct numerical Simulations (DS) model which are taken as reference data. Simulations have been carried out in the temperature field where PCM undergoes phase change transition, but no phase change is applicable for other material. The higher-conductivity phase is an open-cell foam which can be schematically represented as a BCC structure which is considered a most close real foam structure [19].

2. Geometry and thermophysical properties of composite PCMs

The composite PCMs here considered are made of a metallic, open-pore structure filled by a PCM. These composites are modelled considering the porous structure (a foam, for example) as an orderly lattice of inverse Body Centered Cubic cells of the same geometry (see Fig. 1a). The unit cells are characterized by their side length L and sphere diameters d (or, alternatively by the pore volume fraction, ε [12]). The foams are made of commercially pure Al. And the PCM embedded in Al foam is docosane (paraffin wax with $C_{22}H_{46}$), which is characterised by the melting temperature T_m= 317K and the latent heat (LH) of 260 kJ/kg [13,14].

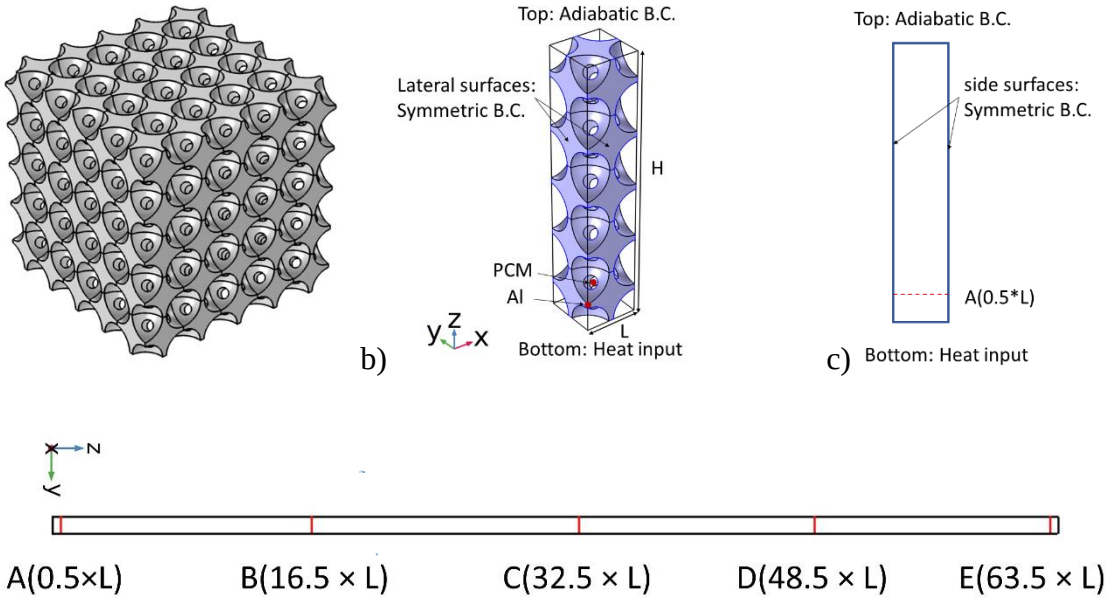

Figure 1 a) Physical model of inverse BCC lattice. Geometrical features and boundary conditions for DS (b) and 1T (c) models. d) z-axis coordinate corresponding to section planes where Al and PCM reference points are taken.

The properties of the Al and PCM phases are shown in Table 1. They have been selected as those in [13,14] to obtain results comparability. In the case of PCM phases, their heat capacity can be described including both specific heat and latent heat of melting, so that the phase transition can be accounted easily. These C_p description can be derived by differential scanning calorimetry measurements [20], or can be simplified by separating the fully solid, fully liquid, and transition temperature range [21]. In the present study, $C_{p,paraffin}$ has been described using the triangular peak description with same value of specific heat $C_{p,\,sol/liq}$ for the fully solid phase and fully liquid phase described by following Eq.1 [21] and shown in Fig 2a. The

corresponding volume fraction of liquid paraffin with temperature can then be derived and plotted in Fig.2a as well.

$$C_{p,\,paraffin}=\begin{cases} C_{p,sol/liq} & T < T_m - b \\ C_{p,sol/liq} + \frac{2\times LH}{b}\left(\frac{T+b-T_m}{b}\right) & T_m - b \le T \le T_m \\ C_{p,sol/liq} & T > T_m \end{cases} \quad (1)$$

where (T_m-b) to T_m is the melting temperature range of the PCM, b is assumed as 2K in the present study. For the specific paraffin considered in the paper, the modelled melting temperature range is thus 316K-318K. By this model the C_p of paraffin assumes a peak value $C_{p,peak}$ at T_m=318K, which is 262.89 kJ/(kg·K).

Different sets of composite PCMs have been considered by varying cell length L or porosity ε. Cell length L is considered to be 0.4, 1, 2, 3, 5 mm, while the volumes fraction of pore ε (corresponding to the volume fraction of PCM) considered is 0.757, 0.8, 0.85, 0.9 and 0.95.

Table 1. Thermophysical properties of interest for Al and PCM phases and the corresponding effective properties for the composite PCMs with the porosity ε used in the article. The first ones are used in DS model, the effective ones are used in 1T model. a) from [13,14], b) calculated.

Material	ρ [kg/m^3]	λ [W/(m·K)]	$C_{p,\,sol/liq}$ [kJ/(kg*K)]	$C_{p,\,max}$ [kJ/(kg*K)]	T_m [K]
Paraffin (PCM)	785 [a]	0.4 [a]	2.89 [a]	262.89 [b]	317 [a]
Al (foam)	2719 [a]	202.4 [a]	0.871 [a]	/	/
Composite PCMs (ε=0.757)	1254.962 [b]	31.157 [b]	1.827 [b]	124.927 [b]	317 [a]
Composite PCMs (ε=0.8)	1171.800 [b]	24.136 [b]	1.953 [b]	141.294 [b]	317 [a]
Composite PCMs (ε=0.85)	1075.100 [b]	16.586 [b]	2.124 [b]	163.490 [b]	317 [a]
Composite PCMs (ε=0.9)	978.400 [b]	9.836 [b]	2.329 [b]	190.074 [b]	317 [a]
Composite PCMs (ε=0.95)	881.700 [b]	4.150 [b]	2.579 [b]	222.489 [b]	317 [a]

3 Mathematical formulation of 1T and DS models

In present study, only heat conduction is considered for both 1-T and DS models. Thus, both 1T and DS models for a composite material made of Al and paraffin phases are based on the energy balance equation:

$$\rho_i C_{p,i} \frac{\partial T_i}{\partial t} - \lambda_i \nabla^2 T_i = 0. \quad (2)$$

where ρ, C_p, λ are the density, specific heat and thermal conductivity of the i phase, respectively. In DS model, two different phases, Al and PCM, are considered (Table 1), with no therma resistance at their interface. The temperature and heat flux is continuous at the interfaces between phases.

On the other hand, the composite PCM is considered as a homogenous material by 1T model, and the effective thermal properties are used for it and described in the following paragraph.

3.1 Effective properties of the composite PCM used in 1T model

The effective properties used for the homogeneous phase considered in 1T model are calculated as follows for thermal conductivity, density and specific heat. For Al-paraffin composites characterized by inverse BCC structure considered in present study, all the effective properties are only related to the phase volume amount (thus to the porosity of the composite PCM), not to the size of unit cells. Thus, values are summarized in Table 1 for each set of porosity values.

For the composite materials, effective thermal conductivity (λ_{eff}) depends on the thermal conductivity, the geometric distribution and the volume fraction of each component [22]. Since λ_{eff} plays a critical role in the thermal response of composite materials [13,14], analytical models for different lattices [14,23] and more general numerical methods like direct simulation (DS) or Lattice Monte Carlo (LMC) [24–26] have been proposed to predict λ_{eff}. Among them, the modified Progelhof model (Eq.3) is presented to estimate λ_{eff} for the Al-paraffin composites characterized by inverse BCC structure and porosity ranging from 0.69 and 0.98 [18].

$$\lambda_{eff}=\varepsilon\times\lambda_{PCM}+(1-\varepsilon)^{1.3296}\times\lambda_{Met} \quad (3)$$

The values of λ_{eff} calculated by Eq.3 are listed in Table 1 for the considered set of porosity values. It decreases from 31.157 W/(m·K) to 4.150 W/(m·K) as porosity increases from 0.757 to 0.95. The λ_{eff} values calculated from the analytical formula Eq.3 are very close to that calculated in Z direction by DS method. As an example of ε=0.757, the values are 31.157 W/(m·K) and 31.229 W/(m·K), respectively.

For a composite PCM, the effective density (ρ_{eff}) can be simply derived by the volume-weighted average of the components' density, while the effective specific heat ($C_{p,eff}$) can be calculated by the mass-weighted average [24]. By using the aforementioned temperature-dependent C_p description for paraffin, the temperature description of $C_{p,eff}$ for composite PCMs can be derived. They are shown in Fig. 2b for the porosity sets considered, and the corresponding $C_{p,max}$, is given in Table 1.

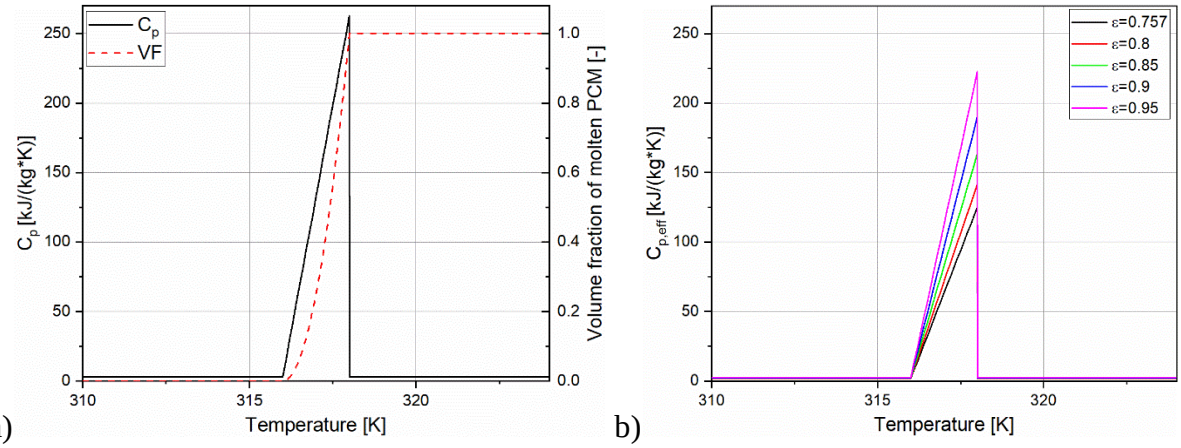

Figure 2 (a) Modelled specific heat and volume fraction (VF) of molten PCM as a function of temperature for the paraffin used as PCM. (b) Effective specific heat of Al-paraffin composite PCMs at varying pore volume fraction of the metallic structure.

3.2 1T and DS implementation

Both DS and 1T models have been implemented in a finite element software. DS model considers 2-phase (the Al and paraffin) system, and its boundary conditions are shown in Fig. 1b. The homogeneous system with effective material properties for 1T model is presented in Fig. 1c, with corresponding boundary conditions. The considered structure is considered to consist in N_c stacked unit cells of side L, where different height $H= N_c \times L$ have been considered, with N_c= 5, 10, 17, 25, 32, 41, 49, 64. For both models, in all the simulated tests performed during the present study, symmetric boundary at lateral surfaces is considered and a homogeneous heat flux is applied at the bottom surface of the modelled structures, while the top surface is thermally insulated (adiabatic).

Due to simple phase arrangement, mapped mesh has been selected for 1T model. The mesh sensitivity analysis has been carried out by considering number of elements for unit cell length of 5, 10, 20. Time sensitivity has been carried out considering time steps of 1,0.1 and 0.01s. The optimal combination is 10 elements per unit cell length (total mesh number is $10 \times 10 \times N_c$) and time step of 0.1s.

The complex porous structure of Al requires a kind of element type able to mesh regardless of structure shape in DS model, that is obtained by the use of free tetrahedral element. The mesh size optimization is carried out for the lower side length and porosity (L=0.4mm, ε=0.757) by fixing minimum mesh size, maximum element growth rate, curvature factor and resolution of narrow regions (1.6×10^{-6} m, 1.4, 0.4, 0.7 respectively) and optimizing the maximum element

size in the range d/50-d/5. Results independent from mesh-size and time step have been obtained when the latter is equal to 0.1s and the maximum mesh size is equal or lower than d/20. These values have been considered for all the simulations for the DS model.

4 Simulation

In order to reach the targets of the present article, 4 sets of simulated tests have been performed, with specific aims, thus each of them has considered one or more specific combinations of porosity, cell coarseness, heat flux, sample height.

In Case 1, a set of tests are to check how, in nonequilibrium conditions, the maximum thermal difference between Al and PCM phases at a specific height is affected by the overall height of the sample. For this reason, tests have been performed by using the only DS model (at the same height, 1T model predicts only 1 temperature, to be considered for both phases). For tests, 4 samples built with the same BCC structure characterized by L = 2mm and ε=0.757 are used. They differ for their overall length H along the Z-direction corresponding to N_c equal to 17, 33, 49, 64 times the cell side L. The boundary conditions are the ones described in paragraph 3.2, where the heat flux q = 10 W/cm^2 is homogeneously supplied at the bottom surface (where Z=0). Reference section planes have been considered at representative sections located at the A (0.5×L), B (16.5×L), C (32.5×L), D (48.5×L) and E (63.5×L). As N_c increases (and thus sample height), the other points C-E are progressively included in the samples. Each of these heights corresponds to a mid-section of the BCC cell, which includes the central point of a PCM sphere (point referred as 'PCM' in Fig. 1b). At these representative sections, the distance from the point PCM to Al/PCM interface is maximum, and the maximum temperature difference within PCM phase is expected. Focusing the attention on Al, the 3- order of magnitude higher thermal conductivity with respect to paraffin makes it possible to consider that in this phase the temperature is homogeneously distributed, so that the maximum temperature at the PCM/Al interface is equal to the one at the core of the Al structure (point referred as 'Al' in Fig. 1b). The temperature difference measured in points Al and PCM in each of the above sections (T_{Al}-T_{PCM}) defines the thermal inhomogeneity in it.

Case 2 is aimed at checking the single and combined impact of heating conditions and coarseness of porous structure on local thermal difference among the reference points identified as Al and PCM. Calculations have been performed by DS model, considering only the highest sample height H=64×L of Case 1, while the cell side L is selected as 0.4mm, 1 mm, 2 mm, 3 mm and 5 mm and the heat flow q is selected as 2 W/cm^2, 4 W/cm^2, 7 W/cm^2 and 10 W/cm^2.

Furthermore, a set of pore volume fractions (porosity) are considered for the metallic structure: ε = 0.757, 0.8, 0.85, 0.9, 0.95.

Case 3 is performed to check if and to what extent the thermal difference at section A, the one closer to the heating surface, is affected by the sample height H, heat flux q and cell side length L. Thus, DS simulated tests have been performed on samples with the same porosity ε=0.757, different side L, (ranging from 0.4mm to 10mm) and different stacked number of unit cells N_c (varying from 5 to 64). In some cases, ε=0.8, 0.85, 0.9 are additionally considered. Similarly, only DS models are carried out. The simulated tests are carried out considering heat flux in the range 1 W/cm^2 to 10W/cm^2.

Case 4 is aimed at comparing the thermal response of the composite PCMs simulated by DS and 1T models. Simulated tests are thus carried out for both models on sample with porous Al structure having the same porosity ε=0.757 and different coarseness, (L=0.4mm, 1mm, 2mm, 3mm and 5 mm). The sample height is H=64×L. For each sample, simulated tests are run for heat flux q= 1 W/cm^2, 2 W/cm^2, 4 W/cm^2, 7 W/cm^2, 10 W/cm^2 (i.e., in positive Z-direction). For each of them, the thermal profiles in sections A-E are derived at reference points for Al and PCM in DS model, while a single temperature profile is obtained in 1T model.

For some simulated DS cases, the local and overall molten PCM volume fraction is calculated as follows. A cubic lattice of 100×100×100 points is overlapped to each unit BCC cell. The points belonging to PCM phase are identified as points NPCM and a temperature profile is derived for each of them. Correspondingly, by means of the correlation between temperature and volume fraction of molten paraffin shown in Fig. 2a, the volume fraction profile of molten PCM is calculated for each point PCM. In 1T model, the calculation of time-dependent volume fraction of molten PCMs is obtained by considering 100 points along the z-direction for each cell side L. And molten PCM volume fraction profiles of each point is derived from its temperature profile by means of the correlation shown in Fig. 2a.

5 Results and discussion

5.1 Case 1: local thermal difference in sections at different height

Simulation results of thermal response have been analyzed at the representative sections mentioned before, located at the A(0.5×L), B(16.5×L), C(32.5×L), D(48.5×L) and E(63.5×L). Due to the different height, only sections A and B are presented in the shortest sample.

Fig.3a displays that temperatures profiles obtained by DS simulations in points Al and PCM at sections A-E for different sample heights referred by the number of stacked cells (17, 33, 49 or 64). In section A that far from the far-boundary for all the samples, the temperature of Al-foam, and PCM for different sample heights are close. In section B, the far-boundary effect is clearly visible for the shortest samples, for which the temperature increase is faster during the heating stage up to the PCM melting temperature range (316K-318K), point PCM stays melting temperature range for a longer time than for other samples, after that increase faster. For the higher samples, the thermal profiles of points Al and PCM in section B are far closer.

A behavior similar to points in section B can be observed for the temperature profiles of reference points at sections C-E for the shortest sample where the reference point (C-E) exists. Lastly, Fig.3a shows that the temperature difference between the reference points Al and PCM reaches maximum close to the end of PCM phase transition, at 318 K, then temperature of point PCM increases sharply. The maximum temperature difference $\delta_{Al\text{-}PCM}$ =max (T_{Al}-T_{PCM}) in a given section can be considered as a measure of the thermal inhomogeneity. $\delta_{Al\text{-}PCM}$ at points A-E is here shown in Fig.3b. It is obvious that, with the exception of the cases for which the reference point (B-E) lays in the BCC cell closest to the adiabatic far-boundary, $\delta_{Al\text{-}PCM}$ differs less than 1 K for different sample height. At point A, $\delta_{Al\text{-}PCM}$ is maximum and close to 10 K for all the sample height. This means that for the relatively high heat flux considered, the temperature differences at the mid-section (A) of the cell closer to the surface where heat flux is applied are not affected by the boundary conditions at the far-end section.

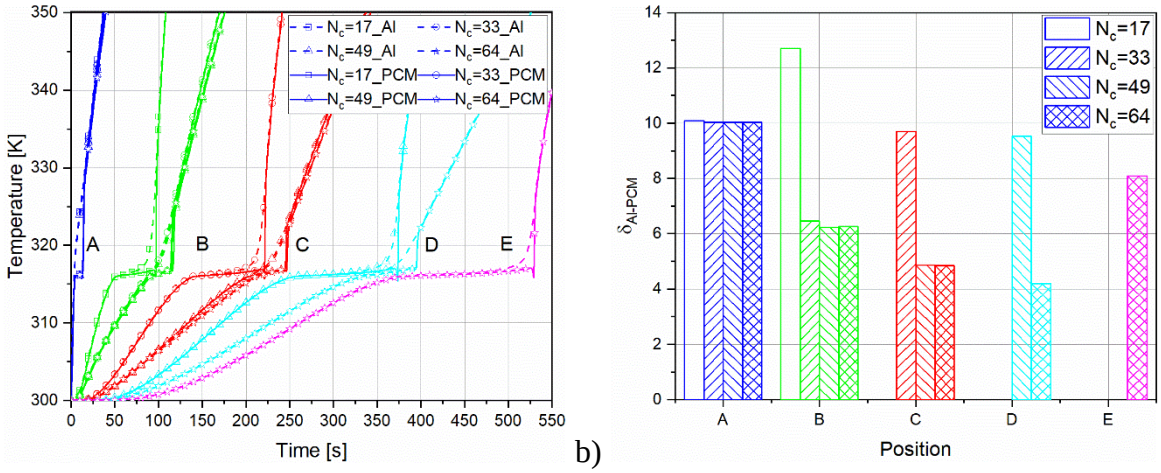

a) b)

Figure 3 a) Comparison between thermal profiles in the centre of the PCM sphere and the core of Al structure at reference section planes A-E supplied by DS model for samples of different height (17, 33, 49, 64 times L) and a constant heat flux of q=10W/cm^2 b) The maximum

temperature difference between Al and PCM at sections A-E ($\delta_{Al\text{-}PCM}$) for samples of different sample height, characterized by the number N_c of stacked cells.

5.2 Case 2: Effect of heat flux and porous material coarseness on local temperature differences.

The results of DS simulated tests performed in case 2 have been analyzed and the maximum temperature difference $\delta_{Al\text{-}PCM} = \max (T_{Al}-T_{PCM})$ between the Al and PCM reference points in each section are shown in Fig.4a at reference points of samples with different side length L (in mm), but a common porosity value $\varepsilon=0.757$. Curves referring to the 4 different values of heat flux considered for this case are presented in different color. The boundary effects at the section closer to the heating and adiabatic ones can be observed, while a roughly linear decrease of $\delta_{Al\text{-}PCM}$ with z- values of considered section can be noted.

The effect of the coarseness of the porous structure on $\delta_{Al\text{-}PCM}$ at given q values is clear, as well as the increase of $\delta_{Al\text{-}PCM}$ with q and L. It has been observed that when $\delta_{Al\text{-}PCM}$ in reference section A is plotted in terms of the product between q and L, an almost linear correlation is observed, as shown in Fig. 4b. The correlation can be written as:

$$\delta_{Al\text{-}PCM} = q \times L/\lambda_{melting} - \theta \quad (4)$$

where $1/\lambda_{melting}$ is the slope of the fitting line and the parameter $\lambda_{melting}$ has been referred as a thermal conductivity due to its unit W/(m·K). And the unit of $\delta_{Al\text{-}PCM}$, L and heat flux q is K, m and W/m^2, respectively. In addition to the above correlation, calculated for $\varepsilon=0.757$, similar ones have been derived for PCM/Al composites characterized by different porosity, as shown in the same Fig. 4b. The fitting constant θ is identified as -0.85 and the calculated $\lambda_{melting}$ range from 20.24 to 9.10 W/(m·K) for ε varying from 0.757 to 0.95 (Fig. 4c), their best-fit correlation being:

$$\lambda_{melting} = -97.874\varepsilon^2+118.55\varepsilon-15.671 \quad (5)$$

Even if $\lambda_{melting}$ decreases as porosity increases, it is not directly correlated to the decrease of λ_{eff} with porosity, since the $\lambda_{melting}/\lambda_{eff}$ ratio varies with ε, as shown in the same Fig. 4c.

The combination of Eq. 4 and Eq. 5 results in the following equation, which enables to derive the maximum temperature difference $\delta_{Al\text{-}PCM}$ at section A as a function of geometrical features (L, ε) and heat flux.

$$\delta_{Al\text{-}PCM} = q \times L/(-97.874\,\varepsilon^2+118.55\varepsilon-15.671)- 0.85 \quad (6)$$

The equation allows to build maps where the iso-temperature difference ($\delta_{Al\text{-}PCM}$) are plotted as a function of the Al material coarseness (L) and the service conditions (q) for a PCM/porous Al structure of a given porosity ε. The map corresponding to ε=0.757 is given in Fig. 4d.

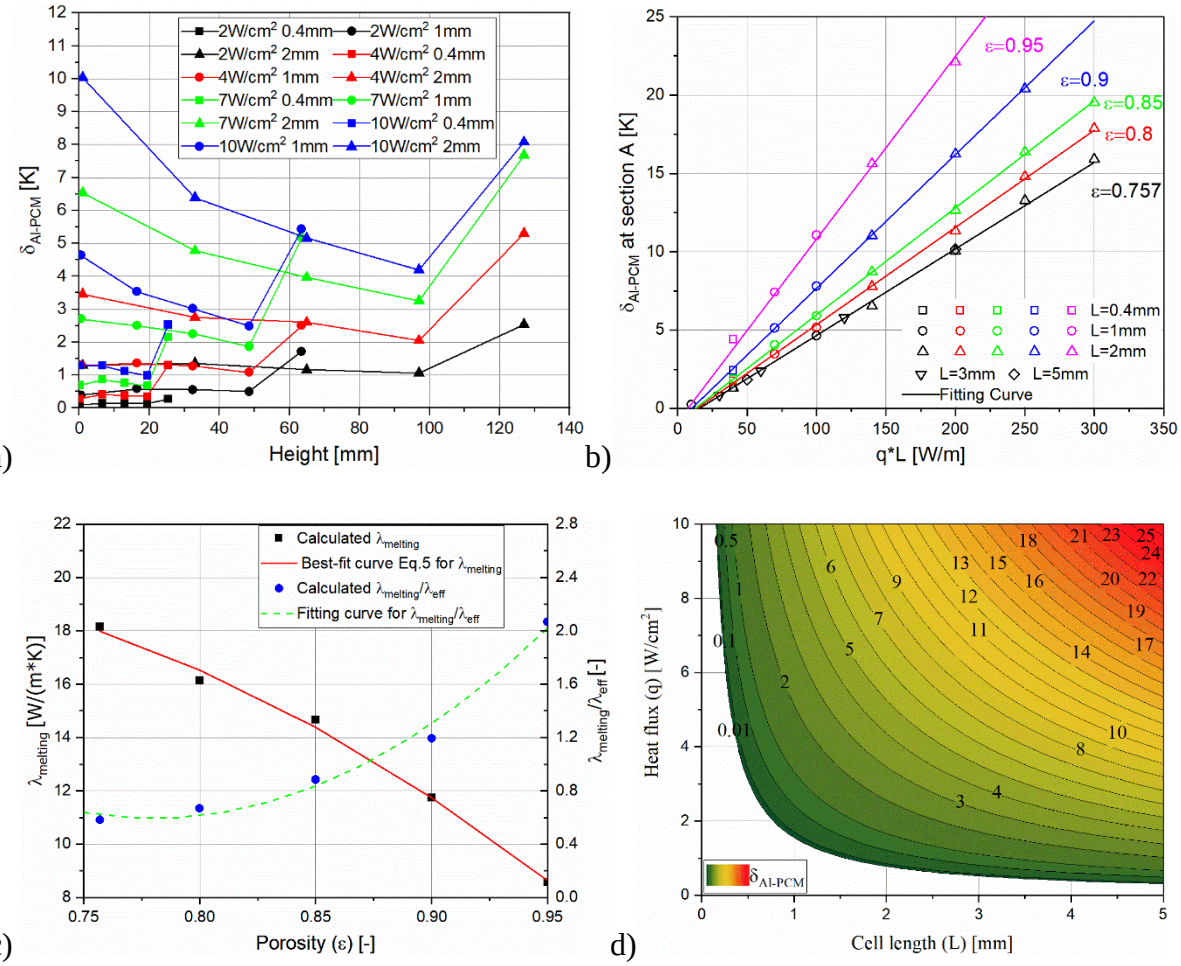

Figure 4 a) Maximum temperature difference $\delta_{Al\text{-}PCM}=\max(T_{Al}-T_{PCM})$ between the representative points for Al and PCM in sections A-E as a function of points distance from the heated surface (Z=0) for different combinations of cell side length L and heat flux q and the same porosity ε=0.757. b) Maximum temperature difference $\delta_{Al\text{-}PCM}$ at point A as a function of the product of cell length L and heat flux q obtained for different porosity values, for each of which a best-fit curve with slope ($1/\lambda_{melting}$) has been derived. c) Correlation of $\lambda_{melting}$ and of $\lambda_{melting}/\lambda_{melting}$ with porosity ε. d) Iso- $\delta_{Al\text{-}PCM}$ curves as a function of the cell side L and heat flux q for PCM/Al porous structures characterized by ε=0.757. Different colors refer to regions where the same maximum difference between Al and PCM temperature is expected. Only situations where $\delta_{Al\text{-}PCM}$>0.01K are colored.

5.3 Case 3: Effect of sample height, structure coarseness and heat flow on local thermal differences

Maximum temperature difference $\delta_{Al\text{-}PCM}$ is plotted (in a logarithmic scale) vs. the number of stacked cells N_c for different combinations of L, q, and a fixed porosity 0.757 in Fig. 5a. It can be observed that $\delta_{Al\text{-}PCM}$ reduces progressively as N_c (and thus the sample height) increases, reaching a stable value above a number hereafter referred as N_s. For a given porosity ε=0.757, the curves corresponding to the same product of q×L (or $\delta_{Al\text{-}PCM}$) are overlapped (see for example the cases of L=0.4mm, q=10W/cm^2 and L=2mm, q=2W/cm^2), and N_s values are shown for each value of $\delta_{Al\text{-}PCM}$ as red star points in Fig. 5a. As a result, N_s can be correlated to $\delta_{Al\text{-}PCM}$. The best-fit curve shown in Fig. 5a has the following equation:

$$N_s = -12.72 \times \ln(\delta_{Al\text{-}PCM}) + 46.02 \qquad R^2 = 0.9876 \qquad (7)$$

The impact of porosity on $\delta_{Al\text{-}PCM}$, shown in Fig.5b, presented that the curves corresponding to the $\delta_{Al\text{-}PCM}$ of about 5 are close for porosity ranging from 0.757 to 0.9, and the same observation is found in the curves corresponding to the $\delta_{Al\text{-}PCM}$ of about 1 for porosity 0.757 and 0.9. It also can be observed that the sample height has a limited effect on $\delta_{Al\text{-}PCM}$ for ε=0.95 and N_s obtained for ε=0.95 is lower than the N_s obtained for the porosity of 0.757 to 0.9. Therefore, $\delta_{Al\text{-}PCM}$ for ε=0.8 to 0.95 can surely reach a stable value when N_c above N_s derived on a basis of ε=0.757.

Thus, Eq.7 also can be used to estimate the N_s for ε=0.757 to 0.95. By combining Eq.6 and Eq.7, N_s can be described as a function of geometrical features (L, ε) and heat flux q, as follows:

$$N_s = -12.72 \times \ln(q \times L/(-97.874\,\varepsilon^2 + 118.55\varepsilon - 15.671) - 0.85) + 46.02 \qquad (8)$$

Eq.8 indicates that Eq.6 derived on the basic of H=64×L also can be applied to estimate the maximum temperature difference at section A near the heating surface of a sample of $H = N_c * L$ when the N_c above N_s.

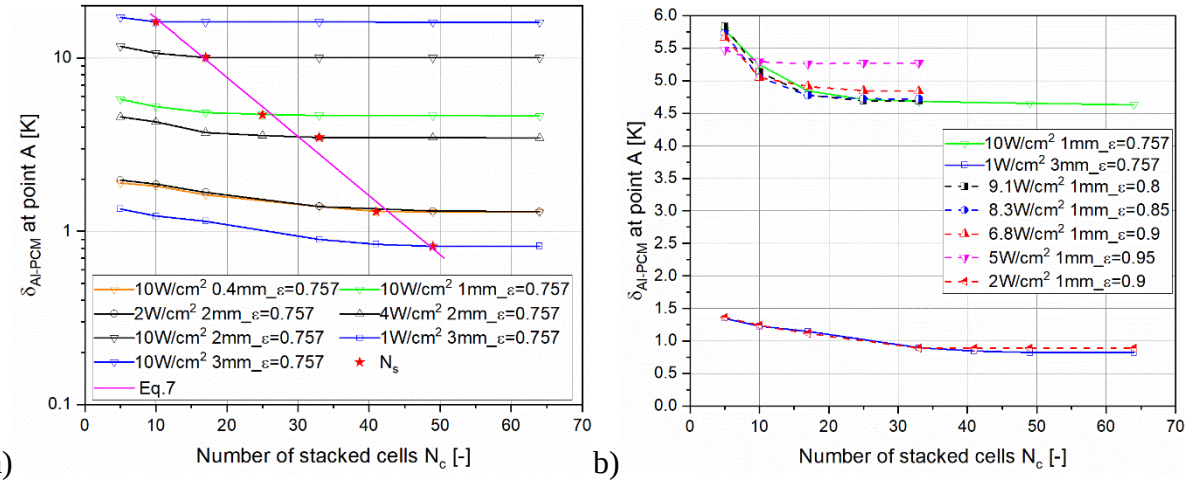

a) b)

Figure 5 Maximum temperature difference between the reference points of Al and PCM in section A as a function of number of stacked cells for different cases of L and q in the case of a) a fixed porosity ε=0.757. Red stars indicate the number of stacked cells (N_s) above which a constant value of $\delta_{Al\text{-}PCM}$ is reached. Best-fit curve for correlation between N_s and $\delta_{Al\text{-}PCM}$ is given by Eq.7. b) porosity ranging from 0.757 to 0.95.

5.4 Case 4 Comparison between results obtained using DS and 1T models.

Comparisons between the results of thermal response of differently modelled composite PCMs have been presented in literature by comparing the progressive increase of the overall volume fraction of molten PCM obtained imposing both constant temperature or constant heat flux on one surface of the samples [13,14] or by comparing the obtained thermal profiles in specific sections [13,14].

5.4.1 Thermal profiles

In the present case 4, comparisons between thermal profiles of differently modelled PCM structures working in different conditions has been considered also for presenting the results of simulated tests in case 4. Fig. 6a and 6b show examples of the thermal profiles in sections A-E obtained at the two reference points referred as Al ($T_{Al,}$) and PCM (T_{PCM}) considered also for previously cases. On the same figures the temperature profiles (T_{1T}) obtained at the same section plane for 1T model are plotted. Since the 1T model considers a homogeneous material, the temperatures are homogeneous within each section plane, due to adopted boundary conditions. Both figures refer to a sample with L=2 mm, ε=0.757, but q = 2 W/cm^2 and 10 W/cm^2, the latter (Fig. 6b) used in case 1. Both figures show that the predictions of the 2 models substantially differ when the temperature at which the PCM starts melting and in a melting

temperature range this difference increases with the heat flux. Looking at the insets of Fig. 6a and 6b, it is clear that the temperature simulated by 1T model lays not only within T_{Al} and T_{PCM} from DS simulations, but that it is closer to T_{Al}.

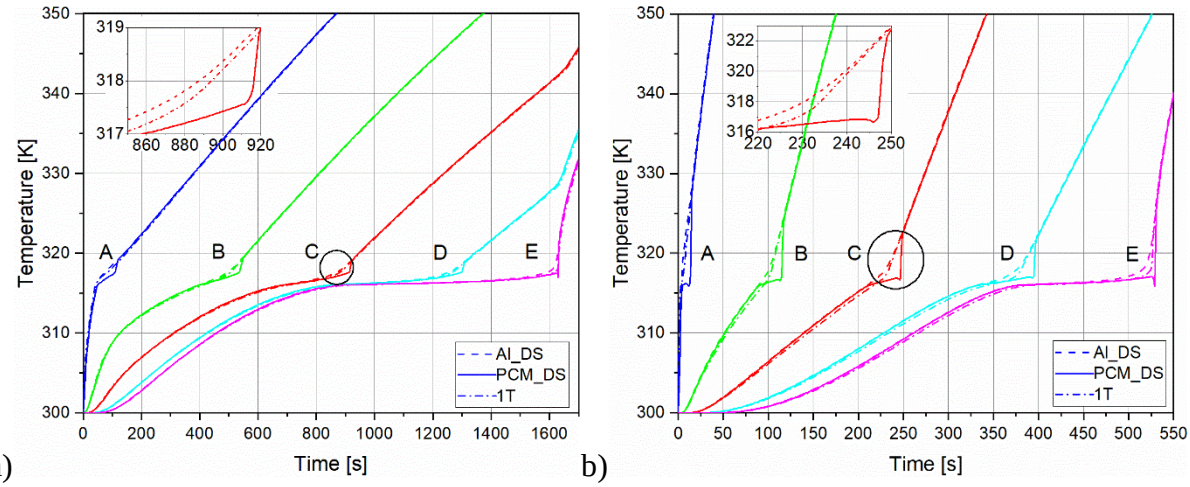

Figure 6 Comparison between temperatures profiles of PCM and Al reference points at sections A-E for DS model and the temperature at corresponding section planes for 1T model. a) L=2mm, q=2W/cm^2; b) L=2mm, q=10W/cm^2.

The situation presented for increasing q value is also observed, as expected, for coarser structures. The authors consider the need of identifying one or a set of parameters in order to compare the predictions obtained by the two models. In the previous cases, the temperature inhomogeneity at constant distance from the sample basis and passing through the center of the inner PCM sphere in BCC cell is characterized by means of parameter $\delta_{Al\text{-}PCM}$ (i.e. the maximum temperature difference between the reference points considered for Al and PCM phases).

In the present case, at sections A-E, the parameters $\delta_{1T\text{-}Al}$ and $\delta_{1T\text{-}PCM}$ are defined as the maximum temperature differences between the temperature at section obtained by 1T model and temperature in the representative points for Al and PCM phases from DS model, respectively. These parameters can be used to compare the differences of thermal profiles produced by the use of DS or 1T models. Fig.7a summarizes the results of the set of simulations carried out for different supplied heat flux values but a constant value of L (2mm). It clearly shows what discussed above by comparing temperature profiles shown in Fig.6, i.e., that δ -values increases as the heating flux increases and $\delta_{1T\text{-}Al}$ is lower than $\delta_{1T\text{-}PCM}$ (maximum at T_m). Further, the effects of heating flux on the δ -values increases as sections considered are closer to the heating surface. Fig.7b shows the changes in terms of $\delta_{1T\text{-}Al}$ and $\delta_{1T\text{-}PCM}$ for different side

length of the metallic structure, the coarser one resulting in larger absolute values of $\delta_{1T\text{-}Al}$ and, particularly, of $\delta_{1T\text{-}PCM}$. Focusing the attention on $\delta_{1T\text{-}PCM}$, it has been done for previous cases, the correlations shown in Fig. 7a and 7b for q and L separately have been checked also for the product of q×L. The result is shown in Fig. 7c. Even these data only refer to the constant porosity ε, a clear dependence of $\delta_{1T\text{-}PCM}$ on q×L exists, similarly to what observed for $\delta_{Al\text{-}PCM}$ in Fig. 4b. Further, the closeness of $\delta_{1T\text{-}PCM}$ to $\delta_{Al\text{-}PCM}$ discussed on the basis of the results in Fig. 4 is confirmed when $\delta_{1T\text{-}PCM}$ is plotted against $\delta_{1T\text{-}PCM}$ in Fig.7d, for several q×L values as well as for several porosity ε in point A. Since $\delta_{1T\text{-}PCM}$, which can be considered as the maximum temperature error in the description of the PCM temperature profile within the PCM phase is only slightly lower than $\delta_{Al\text{-}PCM}$ (representing the actual maximum temperature difference between the temperature of Al, assumed as homogeneous, and the minimum one in PCM phase), $\delta_{Al\text{-}PCM}$ can be used as a parameter suggesting the goodness of 1T model in different situations as far as the porous structure geometry (L, ε) and heat flux are concerned. Thus, the maps derived from Eq. 6 presenting the value of $\delta_{Al\text{-}PCM}$ for a given porosity (and thus a given λ_{eff}, i.e., similar situation in steady-state conditions) as a function of q and L also can be used to suggest the goodness of 1T model.

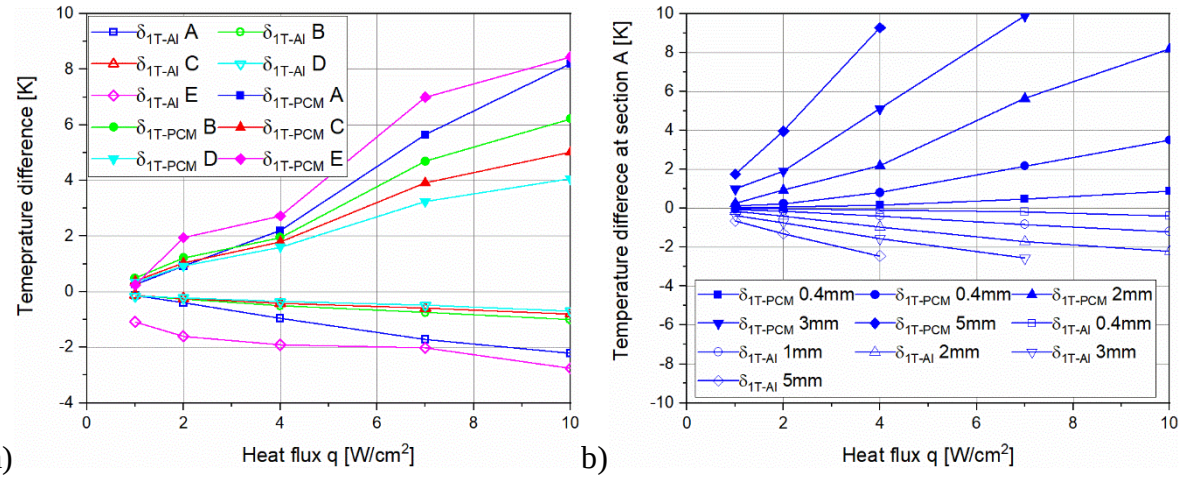

a) b)

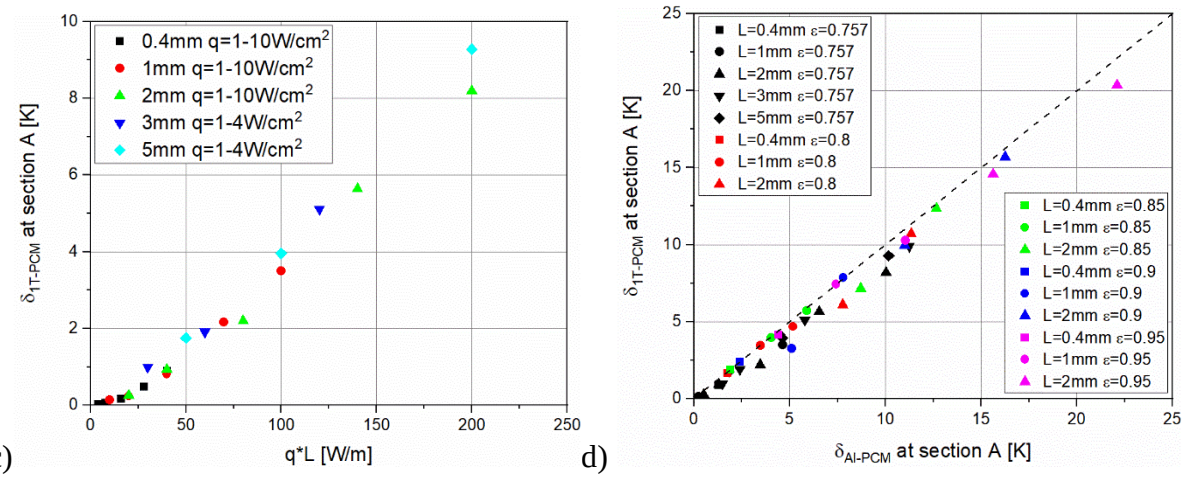

c) d)

Figure 7 The maximum temperature differences $\delta_{1T\text{-}Al}$ and $\delta_{1T\text{-}PCM}$ between DS and 1T model predictions for a) L=2 mm at sections A, B, C, D and E; b) L=0.4 mm, 1 mm, 2 mm, 3 mm and 5 mm at section A. C) $\delta_{1T\text{-}PCM}$ vs. q×L obtained from simulated tests at ε=0.757. d) A correlation of $\delta_{1T\text{-}PCM}$ vs. $\delta_{Al\text{-}PCM}$ for different q, L and ε values.

From the insets of Fig. 6a and 6b, it can be further noted that, in the time range where PCM melting occurs, temperature difference between 1T and Al phase and that between 1T and PCM phase change with time, the first being maximum at the beginning of melting, the second being maximum at the end of it, at T_m. Further, it can be noticed that at times where the end of melting is reached for the reference point PCM (practically, the last point of PCM phases which melts, being located at the center of PCM sphere in the BCC structure), the $\delta_{1T\text{-}PCM}$ is slightly lower than $\delta_{Al\text{-}PCM}$ considered for previous cases. Thus, the considerations done in previous cases to predict $\delta_{Al\text{-}PCM}$ could be applied for the estimation of the goodness of 1T model in terms of temperature predictions. 1T model has more reliable temperature prediction in the case of finer foam structure and lower heat flux supply and $\delta_{1T\text{-}PCM}$ near heating surface has critical value.

5.4.2 Volume fraction of molten PCM.

Since PCMs are typically used for thermal storage application where the amount of stored latent heat where the phase transformation occurs over a narrow temperature range several times higher than the sensible heat accumulated even in a wider temperature range, the amount of heat stored can be considered as roughly proportional to the volume fraction of the molten PCM. The goodness of a model can thus be inferred by the analysis of volume fractions. This can be done also by comparing the results predicted by 1T model with those obtained by DS model, that can be considered as a detailed manner to describe what is going on.

In a composite PCM, the fraction of molten PCM should be evaluated with respect to the total volume fraction of PCM (the porosity ε in the present case). The normalized volume fraction (NVF) of molten PCM is here defined as the ratio between the volume of molten PCM and the volume occupied by PCM for the composite PCM. Both a local and overall approach for the calculation of NVF profiles are possible. l From the practical point of view, in the case of DS model, at each time the volume fractions of molten paraffin at the points NPCM (for the unit cell A-E) have been summed up and divided by NPCM. In the 1T model at each time the volume fractions of the 100 points corresponding to the cell across the considered section A-E are averaged. The overall approach considers the whole sample as the reference volume for the calculation of NVF.

Fig.8a shows the comparison between the local NVF at unit cells A-E and the overall NFV for the sample in the case of L=1mm and q=4W/cm^2 (sample height H=64×L and porosity ε=0.757). It is observed that when the focus is on the description of local phase transition and energy storage, the 2 models significantly differ. Specifically, at each of the unit cell A-E, 1T model predicts longer time for the onset of melting and shorter time for the melting completion. Definitely, 1T model predicts shorter phase transition times, in any case within those predicted by the more reliable DS model.

Fig. 8b shows the comparison between NVF profiles predicted by the two models have also been plotted for effects of q (ranging from 2 W/m^2 to 10 W/m^2) for unit cell A in the case of a sample of L=3mm. In order to quantity the errors induced by the use of 1T model, the maximum difference between NFV predicted by DS and 1T model at this unit cell is considered. In this location the maximum difference can occur both at the onset or offset of the phase transition predicted by 1T model. Nevertheless, since this is a peculiar situation of section A, which could be partly related to its closeness to boundary. Only the temperature difference at the end of the phase transition in 1T model is considered, that is at T_m. The error of NVF caused by 1T model has been calculated for unit cell centered at each reference section as:

$$NVFE = (NVF_{1T} - NVF_{DS})_{Tm} \quad (9)$$

NVFE tends to increase with q, as shown in Fig. 8b. Further, it can be observed that when high heat flux is applied the NVF profile predicted by DS model is not smooth but shows the melting of PCM spheres, that are well visible in the case of a low porosity structure considered for the evaluation here. The volume fraction profiles tend to be smoother as the value of q decreases.

The same occurs when the Al structure coarseness is reduced (i.e., lower L are considered) and when the porosity level is increased.

These errors have been calculated for the unit cell A-E for a selected set of heat flux and sample geometry (varying L but keeping the same porosity and number of stacked cells). The results are shown in Fig. 8c, where NVFE is plotted vs. the product q×L, as done for other cases. The overall trends of the NVFE with the product of q×L is increasing, even if is not linear and monotonic. Further, the differences are particularly high for the unit cell A and E, where boundary conditions effects are present. Here the difference between normalized volume fractions (and thus energy stored) can reach values just below 0.15 for q×L= 8 W/m but increases up to 0.25 when q×L reaches 200 W/m. In internal sections the effect of q×L on NVFE is also remarkable and for the same q×L range it raises from 0.05 to about 0.25.

The overall approach, which has been used by other authors to compare results from 1T and DS models [13,14], give close profiles of NVF (referred as 'Whole sample' in Fig. 8a) and, correspondingly, far lower NVFE, lower than 0.06 for the q×L range considered in Fig. 8b. This confirms that once the predictions of the overall energy stored /released are needed, the 1T model can be considered to supply sufficiently good results.

The NVFE at unit cell A for different porosity versus q×L is plotted in Fig.8d. Even if scattering of result is noticed, a clear correlation between NVFE and q×L can be observed, with the only exception of the results for the highest porosity value (ε=0.95), for which NVFE reaches and holds a constant value of about 0.20 at q×L= 140 W/m.

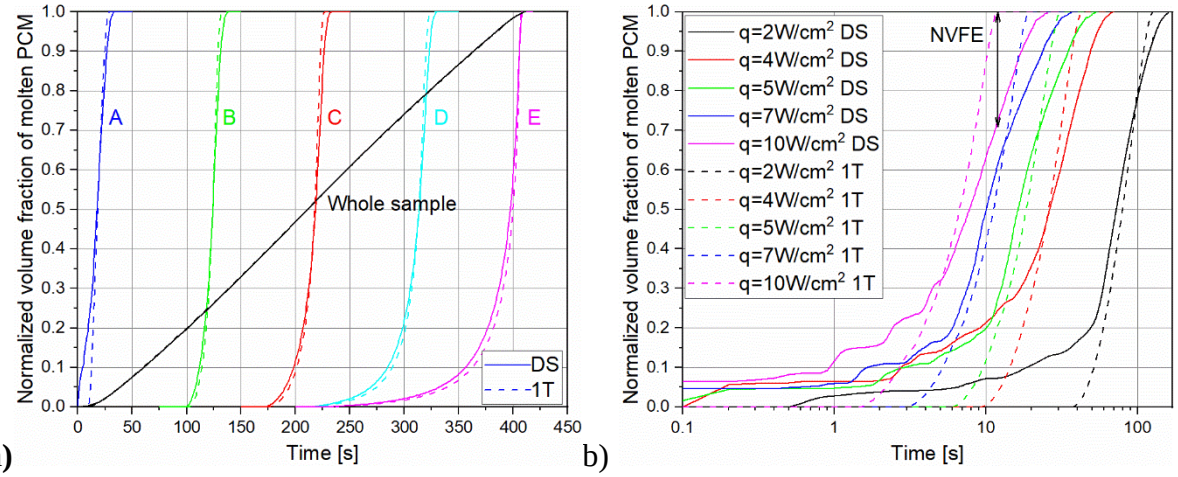

a) b)

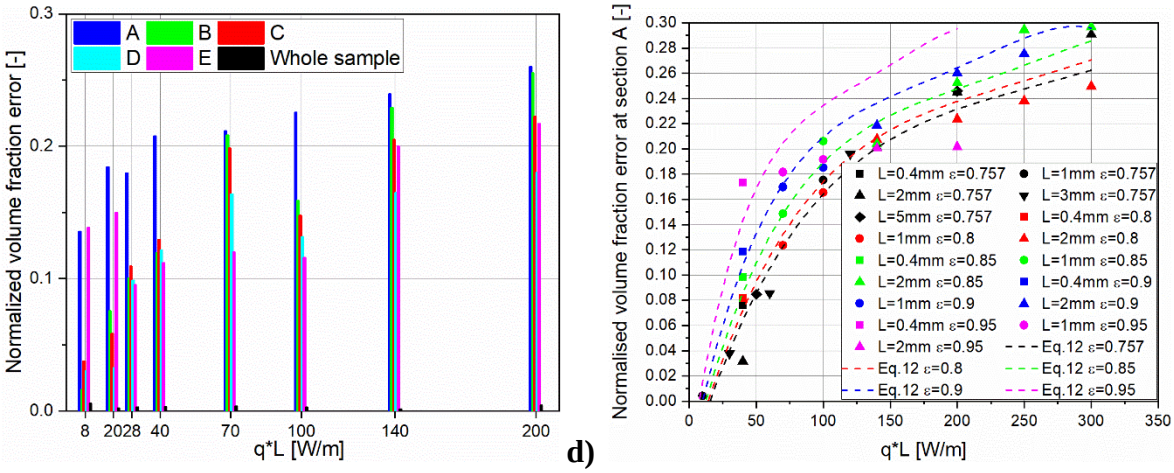

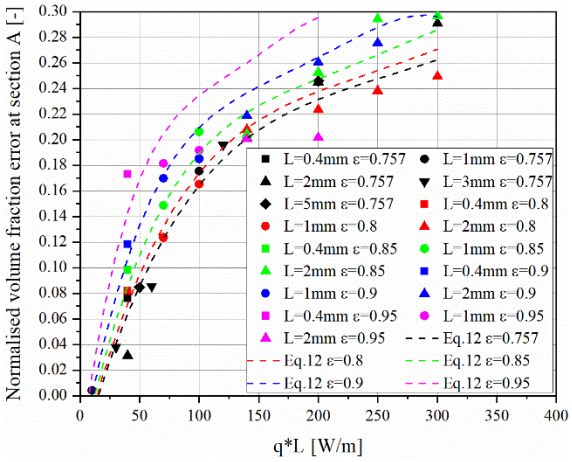

Fig. 8 Comparison between the melting rate of PCM at unit cell A-E and overall volume from direct simulation and the 1T simulation for a) L=1mm, q=4W/cm^2. b) L=3mm, a set of heat flux q=2 W/cm^2 to10 W/cm^2; c) Normalized volume fraction error for a set of q×L for porosity ε=0.757; d) Normalized volume fraction error (NVFE) at unit cell A for a set of q×L for different porosities and NVFE predicted by Eq.12 for different porosities.

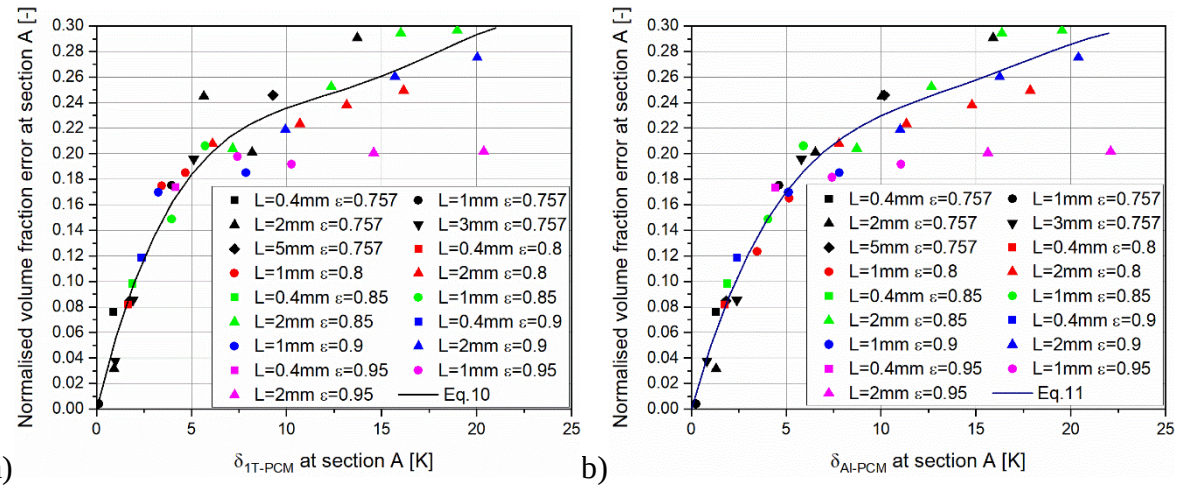

Figure 9. Correlation between NFVE and $\delta_{1T\text{-}PCM}$ (a) and $\delta_{Al\text{-}PCM}$ (b) for different q, L and porosity ε at section A. In each plot, data points calculated for $0.757 \leq \varepsilon \leq 0.9$ have been fitted with a polynomial line.

The final step is to understand the possibility to model adequately the melting of PCM filling a high-conductivity inverse BCC structure with relatively high coarseness and ε on a local scale. Correlations between NFVE and $\delta_{1T\text{-}PCM}$ or $\delta_{Al\text{-}PCM}$ for data points calculated for $0.757 \leq \varepsilon \leq 0.95$, are shown in Fig. 9a and 9b, respectively. For the porosity $0.757 \leq \varepsilon \leq 0.9$ and $\delta_{Al\text{-}PCM}$ and $\delta_{1T\text{-}PCM}$ up to 20K, the following correlations exists:

$$NVFE = -4.73\times10^{-6} \times \delta_{1T\text{-}PCM}^{\ 4} + 2.82\times10^{-4}\ \delta_{1T\text{-}PCM}^{\ 3} - 6.04\times10^{-3}\times \delta_{1T\text{-}PCM}^{\ 2} + 6.05\times10^{-2}\times \delta_{1T\text{-}PCM}; \quad R^2 = 0.95 \qquad (10)$$

$$NVFE = -3.24\times10^{-6} \times \delta_{Al\text{-}PCM}^{\ 4} + 2.03\times10^{-4} \times \delta_{Al\text{-}PCM}^{\ 3} - 4.69\times10^{-3}\times \delta_{Al\text{-}PCM}^{\ 2} + 5.28\times10^{-2}\times \delta_{Al\text{-}PCM}; \quad R^2 = 0.97 \qquad (11)$$

Since, as shown in Fig. 7d, $\delta_{Al\text{-}PCM}$ and $\delta_{1T\text{-}PCM}$ are very close, the only Eq. 11 can be considered. Furthermore, by combining Eq. 6 and Eq. 11, the description of NVFE as function of q×L and ε is obtained as follows.

$$NVFE = -3.24\times10^{-6} \times \left(q\times L/(-97.874\times\varepsilon^2 + 118.55\times\varepsilon - 15.671) - 0.85\right)^4 + 2.03\times10^{-4}\times\left(q\times L/(-97.874\times\varepsilon^2 + 118.55\times\varepsilon - 15.671) - 0.85\right)^3 - 4.69\times10^{-3}\times\left(q\times L/(-97.874\times\varepsilon^2 + 118.55\times\varepsilon - 15.671) - 0.85\right)^2 + 5.28\times10^{-2}\times \left(q\times L/(-97.874\times\varepsilon^2 + 118.55\times\varepsilon - 15.671) - 0.85\right) \qquad (12)$$

Validation of Eq. 12 has been performed by plotting the foreseen NVFE for different q×L values at various porosity ratios in Fig. 8d. It can be observed that Eq. 12 can well predict the NVFE for porosity ε ranging from 0.757 to 0.9 while it overestimates the NVFE for ε=0.95.

As shown in Case 3, the equation can be applied only when the number of stacked cells over N_s defined in Eq. 8. Eq.12 gives the possibility to draw iso-NVFE lines at fixed ε in q vs. L plots, similarly to what done with Eq. 6 in Fig. 4d. This is shown in Fig. 10a and 10b for ε=0.8 and 0.9, respectively. The correlation of NVFE and $\delta_{Al\text{-}PCM}$ has been simply described by parabolic law, which well predicts NVFE by $\delta_{Al\text{-}PCM}$ when $\delta_{Al\text{-}PCM}$ is less than 20K and the corresponding q×L is less than 345 W/m for ε=0.8, less than 245 W/m for ε=0.9. The black area in the upper-right corner of plots in Fig. 10 corresponds to areas where $\delta_{Al\text{-}PCM}$ exceeds 20K. The closer iso-NVFE for ε=0.9 visually suggest the stronger effects of q and L on NVFE.

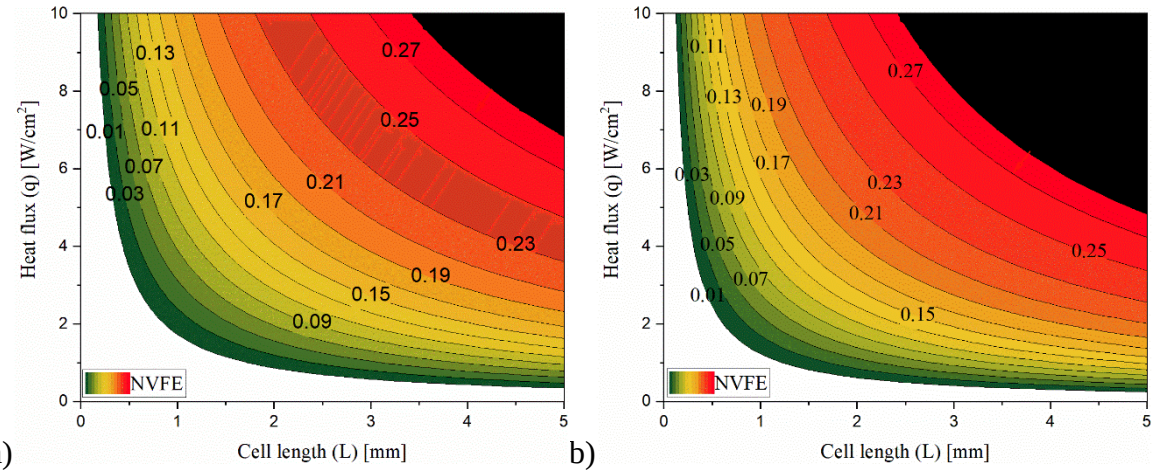

Figure 10. Map showing iso-NVFE curves in section A as functions of q and L for porosity ε= 0.8 (a) and 0.9 (b) derived from Eq. 12. The black area refers to q×L more than 345W/m for ε= 0.8 and 245W/m for ε= 0.9, respectively.

6 Conclusion

The present study has investigated the effect of structure coarseness and boundary condition on local thermal response of the composite PCMs combining paraffin with Al structure modelled as inverse BCC lattice. Local temperature difference at reference points of Al and PCM phases for different height has been presented for a set of cell length L and heat flux q. The exacting correlation between the above temperature difference and the product of L and q have been modelled for pore volume fraction ranging from 0.757 and 0.95. This correlation is applied to the cell closer to heating boundary in case of sufficiently thick specimens (N_c above critical value N_s).

1T model considering homogeneous media with proper effective thermophysical properties, supply good local thermal response predictions for fine structures and lower heat flux input. 1T model is not precise to predict the liquid PCM volume fraction of local section but it is sufficient to estimate the liquid PCM volume fraction of whole sample. A analytical model is proposed to predict the maximum local error for volume fraction of molten PCM, normalized to the overall volume of PCM in the representative unit cell induced by 1T model for the porosity ranging from 0.757 to 0.9.

The main novelty of the paper is the possibility to quantify the error introduced by the use of the simple 1T model in the molten volume fraction prediction (and thus on energy stored/release) for porous Al/paraffic composite PCMs with generic amount of phases, coarseness and service conditions (heat flow).

Acknowledgements

This work was supported by the Italian Ministry for Education, University and Research through the project Department of Excellence LIS4.0 (Integrated Laboratory for Lightweight and Smart Structures).

Reference

[1] K. Pielichowska, K. Pielichowski, Phase change materials for thermal energy storage, Prog. Mater. Sci. 65 (2014) 67–123. doi:10.1016/j.pmatsci.2014.03.005.

[2] W. Su, J. Darkwa, G. Kokogiannakis, Review of solid–liquid phase change materials and their encapsulation technologies, Renew. Sustain. Energy Rev. 48 (2015) 373–391. doi:10.1016/j.rser.2015.04.044.

[3] N. Şahan, H. Paksoy, Novel shapeable phase change material (PCM) composites for thermal energy storage (TES) applications, Sol. Energy Mater. Sol. Cells. 174 (2018) 380–387. doi:10.1016/j.solmat.2017.09.022.

[4] P. Zhang, X. Xiao, Z.W. Ma, A review of the composite phase change materials: Fabrication, characterization, mathematical modeling and application to performance enhancement, Appl. Energy. 165 (2016) 472–510. doi:10.1016/j.apenergy.2015.12.043.

[5] H. Sugo, E. Kisi, D. Cuskelly, Miscibility gap alloys with inverse microstructures and high thermal conductivity for high energy density thermal storage applications, Appl. Therm. Eng. 51 (2013) 1345–1350. doi:10.1016/j.applthermaleng.2012.11.029.

[6] E. Gariboldi, M. Perrin, Metallic Composites as Form-Stable Phase Change Alloys, Mater. Sci. Forum. 941 (2018) 1966–1971. doi:10.4028/www.scientific.net/MSF.941.1966.

[7] G. Wang, G. Wei, C. Xu, X. Ju, Y. Yang, X. Du, Numerical simulation of effective thermal conductivity and pore-scale melting process of PCMs in foam metals, Appl. Therm. Eng. 147 (2019) 464–472. doi:10.1016/j.applthermaleng.2018.10.106.

[8] H. Zheng, C. Wang, Q. Liu, Z. Tian, X. Fan, Thermal performance of copper foam/paraffin composite phase change material, Energy Convers. Manag. 157 (2018) 372–381. doi:10.1016/j.enconman.2017.12.023.

575 [9] X. Xiao, P. Zhang, M. Li, Effective thermal conductivity of open-cell metal foams
576 impregnated with pure paraffin for latent heat storage, Int. J. Therm. Sci. 81 (2014)
577 94–105. doi:10.1016/j.ijthermalsci.2014.03.006.

578 [10] Q. Ren, F. Meng, P. Guo, A comparative study of PCM melting process in a heat pipe-
579 assisted LHTES unit enhanced with nanoparticles and metal foams by immersed
580 boundary-lattice Boltzmann method at pore-scale, Int. J. Heat Mass Transf. (2018).
581 doi:10.1016/j.ijheatmasstransfer.2018.01.046.

582 [11] X. Yang, Z. Guo, Y. Liu, L. Jin, Y.L. He, Effect of inclination on the thermal response
583 of composite phase change materials for thermal energy storage, Appl. Energy. (2019).
584 doi:10.1016/j.apenergy.2019.01.074.

585 [12] Z. Li, E. Gariboldi, Modelling the conditions for natural convection onset in open-cell
586 porous Al/paraffin composite phase change materials: effects of temperature, paraffin
587 type and metallic structure geometry. (Accepted and approved for publication)

588 [13] X. Hu, S.S. Patnaik, Modeling phase change material in micro-foam under constant
589 temperature condition, Int. J. Heat Mass Transf. 68 (2014) 677–682.
590 doi:10.1016/j.ijheatmasstransfer.2013.09.054.

591 [14] X. Hu, H. Wan, S.S. Patnaik, Numerical modeling of heat transfer in open-cell micro-
592 foam with phase change material, Int. J. Heat Mass Transf. 88 (2015) 617–626.
593 doi:10.1016/j.ijheatmasstransfer.2015.04.044.

594 [15] S. Feng, Y. Zhang, M. Shi, T. Wen, T.J. Lu, Unidirectional freezing of phase change
595 materials saturated in open-cell metal foams, Appl. Therm. Eng. 88 (2015) 315–321.
596 doi:10.1016/j.applthermaleng.2014.09.055.

597 [16] X. Yang, W. Wang, C. Yang, L. Jin, T.J. Lu, Solidification of fluid saturated in open-
598 cell metallic foams with graded morphologies, Int. J. Heat Mass Transf. 98 (2016) 60–
599 69. doi:10.1016/j.ijheatmasstransfer.2016.03.023.

600 [17] X. Yang, Q. Bai, Z. Guo, Z. Niu, C. Yang, L. Jin, T.J. Lu, J. Yan, Comparison of
601 direct numerical simulation with volume-averaged method on composite phase change
602 materials for thermal energy storage, Appl. Energy. 229 (2018) 700–714.
603 doi:10.1016/j.apenergy.2018.08.012.

604 [18] P.T. Sardari, H.I. Mohammed, D. Giddings, G.S. Walker, M. Gillott, D. Grant,

Numerical study of a multiple-segment metal foam-PCM latent heat storage unit: Effect of porosity, pore density and location of heat source, Energy. 189 (2019) 116108. doi:10.1016/j.energy.2019.116108.

[19] Z. Li, E. Gariboldi, Review on the temperature-dependent thermophysical properties of liquid paraffins and composite PCMs with metallic porous structures, Mater. Today Energy. (2021) 100642. doi:10.1016/j.mtener.2021.100642.

[20] C. Hasse, M. Grenet, A. Bontemps, R. Dendievel, H. Sallée, Realization, test and modelling of honeycomb wallboards containing a Phase Change Material, Energy Build. 43 (2011) 232–238. doi:10.1016/j.enbuild.2010.09.017.

[21] S. Wang, Y.-Z. Li, Y. Liu, H. Zhou, Y. Li, W. Guo, X. Xiao, Temperature control of permanent-magnet synchronous motor using phase change material, in: 2015 IEEE Int. Conf. Adv. Intell. Mechatronics, IEEE, 2015: pp. 1635–1640. doi:10.1109/AIM.2015.7222778.

[22] D.P.H. Hasselman, L.F. Johnson, Effective Thermal Conductivity of Composites with Interfacial Thermal Barrier Resistance, J. Compos. Mater. 21 (1987) 508–515. doi:10.1177/002199838702100602.

[23] X.H. Yang, J.J. Kuang, T.J. Lu, F.S. Han, T. Kim, A simplistic analytical unit cell based model for the effective thermal conductivity of high porosity open-cell metal foams, J. Phys. D. Appl. Phys. 46 (2013) 255302. doi:10.1088/0022-3727/46/25/255302.

[24] T. Fiedler, I.V. Belova, A. Rawson, G.E. Murch, Optimized Lattice Monte Carlo for thermal analysis of composites, Comput. Mater. Sci. 95 (2014) 207–212. doi:10.1016/j.commatsci.2014.07.029.

[25] H. Ye, Q. Ni, M. Ma, A Lattice Monte Carlo analysis of the effective thermal conductivity of closed-cell aluminum foams and an experimental verification, Int. J. Heat Mass Transf. 86 (2015) 853–860. doi:10.1016/j.ijheatmasstransfer.2015.03.070.

[26] Z. Li, E. Gariboldi, Reliable estimation of effective thermal properties of a 2-phase material by its optimized modelling in view of Lattice Monte-Carlo simulation, Comput. Mater. Sci. 169 (2019) 109125. doi:10.1016/j.commatsci.2019.109125.